The Astrophysical Journal, 785:93 (10pp), 2014 April 20 doi:10.1088/0004-637X/785/2/93
© 2014. The American Astronomical Society. All rights reserved. Printed in the U.S.A.

# LIMITS ON STELLAR COMPANIONS TO EXOPLANET HOST STARS WITH ECCENTRIC PLANETS

Stephen R. Kane[1], Steve B. Howell[2], Elliott P. Horch[3], Ying Feng[4,5], Natalie R. Hinkel[1], David R. Ciardi[6], Mark E. Everett[7], Andrew W. Howard[8], and Jason T. Wright[4,5]
[1] Department of Physics & Astronomy, San Francisco State University, 1600 Holloway Avenue, San Francisco, CA 94132, USA; skane@sfsu.edu
[2] NASA Ames Research Center, Moffett Field, CA 94035, USA
[3] Department of Physics, Southern Connecticut State University, New Haven, CT 06515, USA
[4] Department of Astronomy and Astrophysics, Pennsylvania State University, 525 Davey Laboratory, University Park, PA 16802, USA
[5] Center for Exoplanets & Habitable Worlds, Pennsylvania State University, 525 Davey Laboratory, University Park, PA 16802, USA
[6] NASA Exoplanet Science Institute, Caltech, MS 100-22, 770 South Wilson Avenue, Pasadena, CA 91125, USA
[7] National Optical Astronomy Observatory, 950 N. Cherry Ave, Tucson, AZ 85719, USA
[8] Institute for Astronomy, University of Hawaii, Honolulu, HI 96822, USA
*Received 2014 January 2; accepted 2014 February 25; published 2014 March 31*

## ABSTRACT

Though there are now many hundreds of confirmed exoplanets known, the binarity of exoplanet host stars is not well understood. This is particularly true of host stars that harbor a giant planet in a highly eccentric orbit since these are more likely to have had a dramatic dynamical history that transferred angular momentum to the planet. Here we present observations of four exoplanet host stars that utilize the excellent resolving power of the Differential Speckle Survey Instrument on the Gemini North telescope. Two of the stars are giants and two are dwarfs. Each star is host to a giant planet with an orbital eccentricity >0.5 and whose radial velocity (RV) data contain a trend in the residuals to the Keplerian orbit fit. These observations rule out stellar companions 4–8 mag fainter than the host star at passbands of 692 nm and 880 nm. The resolution and field of view of the instrument result in exclusion radii of 0.″05–1.″4, which excludes stellar companions within several AU of the host star in most cases. We further provide new RVs for the HD 4203 system that confirm that the linear trend previously observed in the residuals is due to an additional planet. These results place dynamical constraints on the source of the planet's eccentricities, place constraints on additional planetary companions, and inform the known distribution of multiplicity amongst exoplanet host stars.

*Key words:* planetary systems – stars: individual (HD 4203, HD 168443, HD 1690, HD 137759) – techniques: high angular resolution – techniques: radial velocities

*Online-only material:* color figure

## 1. INTRODUCTION

Of the confirmed exoplanets, over 500 have been discovered using the radial velocity (RV) technique. A particular attribute of the RV systems is that they preferentially are harbored by bright host stars because of the target selection techniques and the signal-to-noise requirements of the surveys. The advantage of this magnitude bias is that it enables further follow-up and characterization studies of both the star and the harbored planets.

It has been well established that stars in the solar neighborhood have a high rate of stellar multiplicity. This nearby multiplicity rate has been primarily determined through spectroscopic means. Abt & Levy (1976) determined that binary and multiple stars systems are more common than single stars, with a vast majority of their stellar sample showing evidence of stellar companions. Their relatively high rate of stellar multiplicity was revised to a smaller value by Duquennoy & Mayor (1991) in their distance-complete survey of nearby solar-type stars. They found the distribution of solar-type binaries to have a period distribution peak near 10,000 days (30 yr, which corresponds to about 10 AU). A more recent multiplicity survey by Raghavan et al. (2010) found a similar rate of stellar companions to solar-type stars as found by Duquennoy & Mayor (1991).

Planets have been shown to be common from a variety of sources, such as microlensing experiments (Cassan et al. 2012) and Kepler transiting planets (Dressing & Charbonneau 2013). However, relatively few of the known exoplanet host stars have detected stellar companions, and studies have indeed found the multiplicity rate to be lower than the general stellar population (Roell et al. 2012). Clearly there is an inconsistency between the rate of stellar multiplicity of exoplanet host stars and the general stellar population, as discussed above. The presence of stellar companions can have significant implications for planet formation scenarios and the subsequent properties of the systems, such as the period–mass (Zucker & Mazeh 2002) and period–eccentricity (Eggenberger et al. 2004) distributions. Thus, it is of vital importance to clearly establish the true rate of stellar multiplicity amongst exoplanet host stars.

There have been several previous studies that have conducted searches for stellar companions. Bergfors et al. (2013) used lucky imaging to conduct such a search around relatively faint transiting planet host stars. The resolution of their observations allowed the detection of companions 4 mag fainter at 0.″5 separation. Eggenberger et al. (2007) conducted a survey of southern exoplanet host stars using VLT/NACO and were able to detect a handful of previously unknown companions to some of the exoplanet host stars. Attempts are also underway to detect stellar companions to exoplanet host stars that exhibit a linear trend in the RV data (Crepp et al. 2012, 2013).

Here we present the results of high-resolution imaging of four exoplanet host stars with known RV linear trends in the residuals in order to detect or constrain the presence of stellar companions. We also present new Keck/HIRES RV data for HD 4203 that confirm a second planet in that system. Imaging observations were carried out using the Differential Speckle Survey Instrument (DSSI) on Gemini North, a system that

**Table 1**
Star and Inner Planet Parameters

| Parameter | HD 4203b[a] | HD 168443b[b] | HD 1690b[c] | HD 137759b[d] |
|---|---|---|---|---|
| Distance (pc)[e] | $77.2^{+6.7}_{-5.7}$ | $37.43^{+0.99}_{-0.94}$ | $310^{+250}_{-96}$ | $31.027^{+0.097}_{-0.096}$ |
| $V$ mag | 8.70 | 6.92 | 9.17 | 3.29 |
| [Fe/H] (dex)[f] | 0.41 | 0.06 | −0.32 | 0.08 |
| $M_\star$ ($M_\odot$) | $1.13^{+0.028}_{-0.1}$ | $0.995 \pm 0.019$ | $1.09 \pm 0.15$ | 1.4 |
| $P$ (days) | $431.88 \pm 0.85$ | $58.11247 \pm 0.0003$ | $533.0 \pm 1.7$ | $510.88 \pm 0.15$ |
| $T_p$ (JD-2,440,000) | $11918.9 \pm 2.7$ | $15626.199 \pm 0.024$ | $14449.0 \pm 5.0$ | $12013.94 \pm 0.48$ |
| $e$ | $0.519 \pm 0.027$ | $0.52883 \pm 0.00103$ | $0.64 \pm 0.04$ | $0.7261 \pm 0.0061$ |
| $\omega$ (deg) | $329.1 \pm 3.0$ | $172.923 \pm 0.139$ | $122.0 \pm 8.0$ | $88.7 \pm 1.4$ |
| $K$ (m s$^{-1}$) | $60.3 \pm 2.2$ | $475.133 \pm 0.9102$ | $190.0 \pm 29.0$ | $299.9 \pm 4.3$ |
| $M_p \sin i$ ($M_J$) | $2.08 \pm 0.116$ | $7.66 \pm 0.098$ | $6.1 \pm 0.9$ | 10.3 |
| $a$ (AU) | $1.165 \pm 0.022$ | $0.2931 \pm 0.00181$ | $1.30 \pm 0.02$ | 1.34 |
| Slope (m s$^{-1}$ yr$^{-1}$) | $-4.38 \pm 0.71$ | $-3.17 \pm 0.09$ | $-7.2 \pm 0.4$ | $-13.8 \pm 1.1$ |

**Notes.**
[a] Butler et al. (2006).
[b] Pilyavsky et al. (2011).
[c] Moutou et al. (2011).
[d] Zechmeister et al. (2008).
[e] van Leeuwen (2007).
[f] See Section 7.

has already been successfully used to observe much fainter stars in the Kepler and CoRoT fields (Horch et al. 2012). Each of the four target systems in this study harbor a giant planet in an eccentric orbit whose eccentricity may in part be explained by the perturbing influence of the third body. Two of the stars are giants and two are dwarfs. In Section 2, we describe in detail the science motivation behind the selection of the four targets and their relevant properties. In Section 3, we present new RV data that confirm the linear trend for HD 4203 is due to an additional planet in that system. Section 4 outlines the DSSI observations and data reduction processes. In Section 5, we present the results of the imaging data and subsequent constraints on companions in terms of Δ magnitude and angular separation. We map these results in Section 6 to constraints on companions in terms of stellar mass and physical separation. Section 7 briefly describes stellar abundances for the targets in the context of stellar companions and exoplanet orbital eccentricity. Finally, we provide concluding remarks in Section 8, commenting on the implications for limits on stellar and planetary companions in these systems.

## 2. TARGET SELECTION

Our observations were scheduled to occur during the 2013B semester on Gemini North, during which the DSSI instrument (described in Section 4) was deployed as a visiting instrument. We thus selected targets within a right ascension (R.A.) range of $15h < \text{R.A.} < 03h$ and a declination (decl.) range of $-10^\circ < \text{decl.} < +70^\circ$. The targets in our list have all been the subject of RV studies from which their known planetary companions were detected. We elected to focus our observations on bright stars ($V < 12$) with at least one planet in a highly eccentric ($e > 0.5$) orbit. Furthermore, we required that there be no known binary companion to the host star but an RV trend present in the residuals of the Keplerian planetary fit to the data. The above criteria were applied to the known stellar and planetary parameters using the data stored in the Exoplanet Data Explorer[9] (Wright et al. 2011). This resulted in our final list of targets, which includes HD 4203, HD 168443, HD 1690, and HD 137759 (iota Draconis).

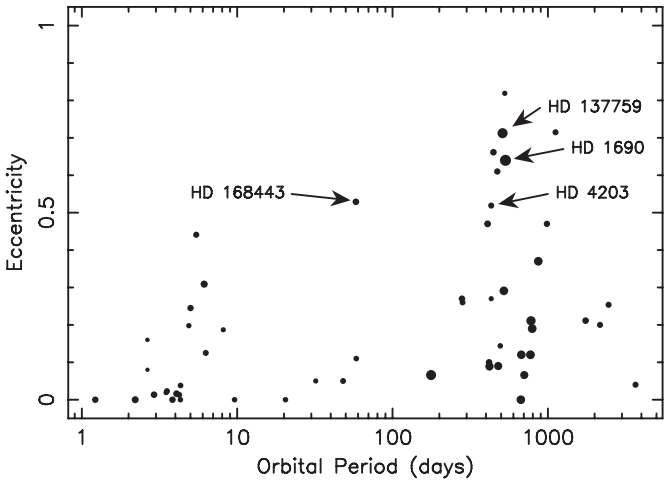


**Figure 1.** Plot of eccentricity vs. orbital period (inner planet) for all systems that are known to have a radial velocity trend in the Keplerian orbital solution and are not known to have a stellar companion to the host star. The size of each plotted point is logarithmically proportional to the radius of the host star to distinguish dwarfs from giants. The locations of the four systems studied in this paper are labeled.

The Keplerian orbital solutions for the four planets/systems along with relevant stellar parameters and references are shown in Table 1. Note that the HD 168443 system has two known planets, and thus the Keplerian orbital solution applies to the b planet. The HD 4203 system also has two planets that are described further in Section 3. The effective search radius for DSSI is 0.″05–1.″4. This means, for example, stars located at 30 pc have a search radius of 1.5–42 AU. As noted above, we selected stars with eccentric planets since a primary motivation is to explore the possibility of scenarios that include a perturbing body that has exchanged angular momentum from the eccentric planet. We also chose to select two dwarf stars (HD 4203 and HD 168443) and two giant stars (HD 1690 and HD 137759) to investigate these scenarios for a range of luminosity classes. Many of these criteria are summarized in Figure 1, which shows

[9] http://exoplanets.org/

**Table 2**
Radial Velocities for HD 4203 from Keck

| Time (JD-2,440,000) | Velocity (m s$^{-1}$) | Uncertainty (m s$^{-1}$) |
|---|---|---|
| 11757.122 | 6.0021463 | 1.31503 |
| 11792.972 | 6.8441796 | 1.58321 |
| 11882.835 | 42.293574 | 1.39100 |
| 11883.848 | 47.667231 | 1.63549 |
| 11900.838 | 76.619395 | 1.28310 |
| 12063.126 | 18.041178 | 1.52620 |
| 12065.129 | 30.488276 | 1.90241 |
| 12096.114 | 19.101145 | 1.47675 |
| 12097.068 | 20.965464 | 1.80766 |
| 12128.116 | 14.444193 | 1.65465 |
| 12133.056 | 15.628565 | 1.49746 |
| 12133.926 | 13.116808 | 1.57353 |
| 12162.918 | 3.3657251 | 1.56790 |
| 12187.962 | 0.90439083 | 1.44404 |
| 12515.017 | 19.283503 | 1.52212 |
| 12535.989 | 11.405924 | 1.52340 |
| 12574.784 | 9.5314431 | 1.95447 |
| 12806.126 | 104.74114 | 1.46572 |
| 12897.903 | 27.623347 | 1.43196 |
| 13180.122 | 24.839053 | 1.36543 |
| 13723.747 | 48.697809 | 0.935456 |
| 13751.749 | 28.752323 | 0.899553 |
| 13752.814 | 31.586298 | 0.921903 |
| 13961.019 | −18.960217 | 1.02713 |
| 13981.909 | −23.106548 | 0.888949 |
| 14339.103 | −18.116657 | 1.00089 |
| 14343.931 | −24.443002 | 0.956635 |
| 14397.802 | −24.972989 | 0.961509 |
| 14430.763 | −22.894478 | 0.985528 |
| 14806.840 | −30.759572 | 1.13911 |
| 15189.785 | −28.156682 | 0.965326 |
| 15381.079 | 6.1080502 | 0.933918 |
| 15414.027 | 66.112621 | 1.01668 |
| 15435.044 | 52.387934 | 1.03033 |
| 15522.893 | −9.1774166 | 1.05714 |
| 15806.918 | −19.001478 | 0.988947 |
| 16112.131 | −31.595639 | 0.991987 |
| 16472.128 | −17.945240 | 0.939638 |

a plot of orbital eccentricity versus orbital period (of the inner planet) for those systems that have a known RV trend but no known stellar companion to the host star. The size of each data point is logarithmically proportional to the radius of the host star. The four targets selected for observations are appropriately labeled and shows that many of the eccentric planets in this population fall in the 400–1000 day period range. The HD 168443 system is an outlier in this plot and thus represents a significantly different system architecture than the other three.

## 3. AN UPDATE TO THE HD 4203 PLANETARY SYSTEM

We present an updated fit to HD 4203b with additional RVs from HIRES at the Keck Observatory (Vogt et al. 1994). Since the work of Vogt et al. (2002) and Butler et al. (2006), we have monitored HD 4203 up to mid-2013. Table 2 lists the 38 HIRES RV observations. We found that the previously identified trend was due to an outer planet. HD 4203c has a period of ∼18.2 yr and a minimum mass of ∼2.17 $M_{\rm Jup}$. Table 3 lists the orbital parameters of HD 4203b and HD 4203c. We fit Keplerian orbits to the RV data with the RVLIN package (Wright & Howard 2009), and we applied a stellar jitter of 4 m s$^{-1}$ Butler et al. (2006). We derived uncertainties for the parameters using BOOTTRAN, the bootstrapping package described by Wang et al. (2012). The combined system fit, RV residuals, and fits for each planet are shown in Figure 2.

**Table 3**
Orbital Parameters of the HD 4203 Planetary System

| Parameter | | HD 4203b | HD 4203c |
|---|---|---|---|
| $P$ | days | $437.05 \pm 0.27$ | $6700 \pm 4500$ |
| $T_p$ | JD-2,440,000 | $11911.52 \pm 2.38$ | $16000 \pm 9600$ |
| $e$ | | $0.52 \pm 0.02$ | $0.24 \pm 0.13$ |
| $\omega$ | (deg) | $328.03 \pm 2.9$ | $224 \pm 48.8$ |
| $K$ | (m s$^{-1}$) | $52.82 \pm 1.5$ | $22.20 \pm 3.707$ |
| $M_p \sin i$ | ($M_J$) | $1.82 \pm 0.05$ | $2.17 \pm 0.52$ |
| $a$ | (AU) | $1.1735 \pm 0.0222$ | $6.95^{+1.93}_{-0.56}$ |
| RMS | (m s$^{-1}$) | 3.93 | |
| $\chi^2_\nu$ | | 0.87 | |

Because the orbit of HD 4203c has not completed, BOOTTRAN by itself could not constrain well the period, $P_c$, and minimum mass, $M_c \sin i_c$. We also treated the RVs taken before and after the HIRES upgrade in 2004 separately, which results in an offset between the two streams of velocities. In order to constrain the period and mass, we constructed a $\chi^2$ map for the best-fit Keplerian orbits where we fixed values of $P_c$ and $M_c \sin i_c$ at each point in the map. We let all other parameters float, giving us a total of 10 free parameters: 5 for planet b, 3 for planet c, $\gamma$ for the system, and offset between the 2 RV streams. When the offset was a floating parameter in our fitting, we found parameters were not well constrained. Therefore, we enforced a penalty for the values of offset from our fits to obtain the $\chi^2$ map shown in Figure 3.

We first had to determine the offset penalty term. To do so, we identified a pool of Keck stars with similar temperature and gravity as HD 4203 using $\Delta T_{\rm eff} = 225$ K and $\Delta \log g = 0.3$. Within that pool, we filtered out the stars with less than 10 observations for both pre- and post-2004 RVs. We then examined the RV curve of each star to exclude stars that have significant trends or known long-period planets. For stars with planets that are in short orbits (<1 yr), we subtract the orbital solution. We calculated the offset as the difference in mean of the pre- and post-2004 streams. This selection yielded a list of 42 stars for which we calculated the individual offsets and the weighted mean and variance of all the offsets. We plot the distribution of offsets from our list of 42 stars (see Figure 4).

We created the offset-penalized $\chi^2$ map from an array of 101 offset values between −10 m s$^{-1}$ and 10 m s$^{-1}$. Each offset had a corresponding 50 × 50 $\chi^2$ map. Next, we applied each offset to the series of RVs taken after 2004. The penalty term we add to each map is given by $(o-\mu_{\rm w})^2/\sigma_o^2$, where $o$ is the corresponding offset, and $\mu_{\rm w}$ and $\sigma_o^2$ are the weighted mean and variance of the offsets from the selected set of stars. For each pixel, we selected the minimum $\chi^2$ value from the stack of 101 offsets. The minima for all the stacks made up the offset-penalized $\chi^2$ map. We also marked contours of the $1\sigma$, $2\sigma$, and $3\sigma$ confidence levels (calculated as $\chi^2 = \chi^2_{\rm min} + \{2.30, 6.17, 11.8\}$) for the two-dimensional $\chi^2$ distribution (Press et al. 2002).

In addition to each of the 101 maps, we ran BOOTTRAN. Every orbital parameter had a structure 1000 × 101 in dimension from the BOOTTRAN runs and the range of offsets. We implemented a two-level mask that first randomly excluded

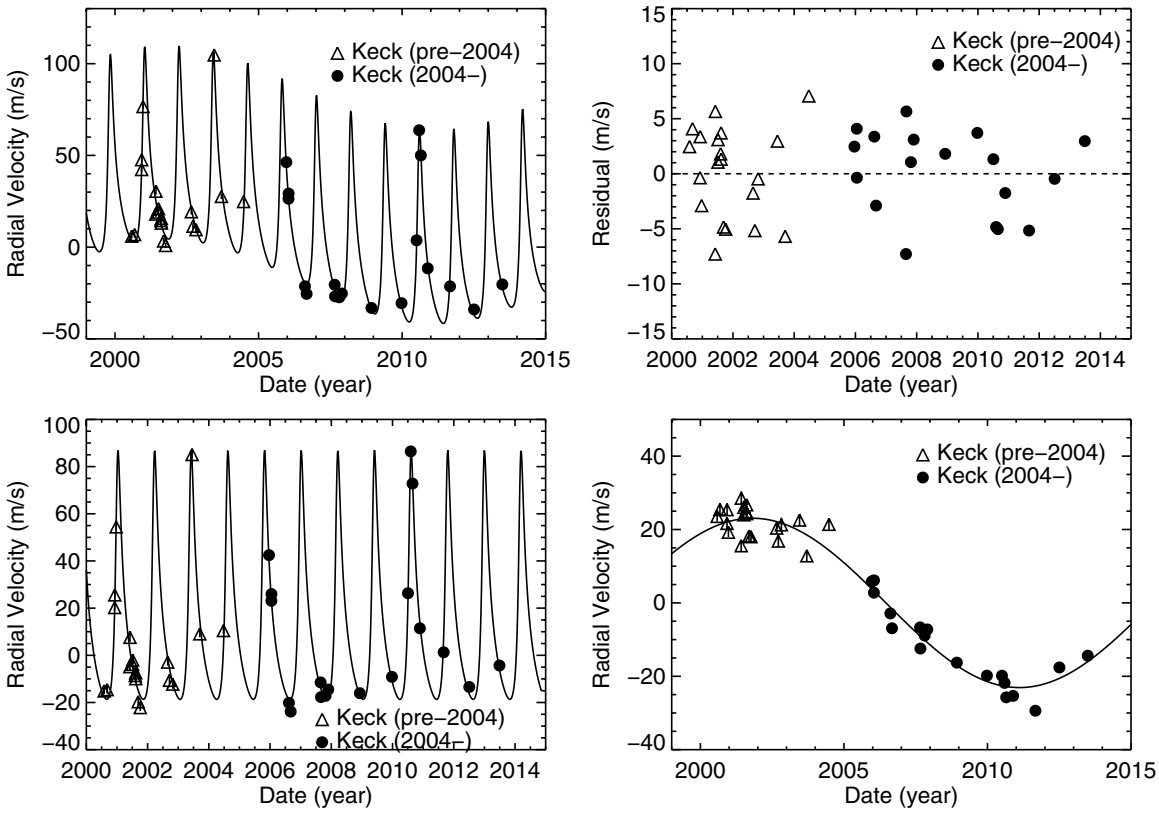


**Figure 2.** Radial velocity and Keplerian fits for the HD 4203 system. In all plots, triangles represent pre-2004 Keck RVs and filled circles represent post-2004 Keck RVs. Solid lines represent the best-fit Keplerian orbits. Top left: Keck RVs overplotted by the best-fit two-planet Keplerian model. Top right: residuals of the RVs with the best-fit two-planet Keplerian model subtracted. Bottom left and bottom right: the RV curves for HD 4203b and c, respectively. We implemented a best-fit offset of 2.38 m $s^{-1}$ in plotting these figures.

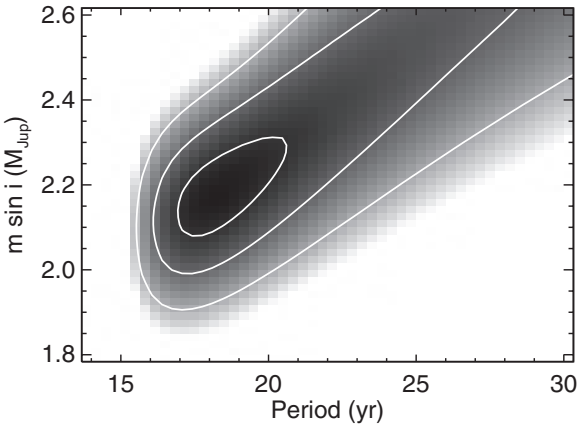


**Figure 3.** Best-fit $50 \times 50$ $\chi^2$ map for fixed values of $P_c$ and $M_c \sin i_c$, with the offset penalty applied. This confirms that the period and mass are constrained to $1\sigma$. We have illustrated the contours of the $1\sigma$, $2\sigma$, and $3\sigma$ (defined by $\chi^2 = \chi^2_{\rm min} + \{2.30, 6.17, 11.8\}$) confidence levels.

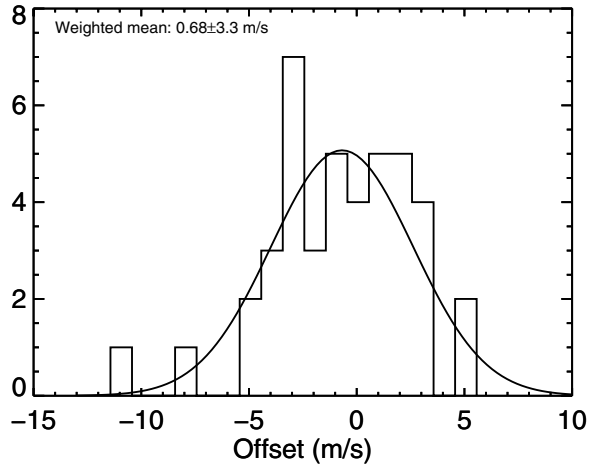


**Figure 4.** Histogram distribution of offsets for 42 stars from the Keck catalog. We selected the stars on the basis of similarity to HD 4203, where $\Delta T_{\rm eff} < 225$ K and $\Delta \log g < 0.3$. We excluded stars that exhibited trends or are known hosts of long-period (>1 yr) planets, and stars that have less than 10 observations for both the pre- and post-2004 RV streams. We calculated the offset for each star's set of RVs and found a weighted mean of $-0.68$ m $s^{-1}$ and a variance of 10.91. We overplot a Gaussian with the same mean and variance.

points less than the weight set by the offset distribution in Figure 4, normalized to 1. Second, we masked out fits that returned a period of 100 yr, which indicates that the fit failed. Using the mask, we created distributions of values for each parameter and determined the width, which was used for the uncertainty. The minimum mass required separate calculation, and we generated an array of $M_c \sin i_c$ on the basis of the distributions of period, velocity semiamplitude, eccentricity, and mass of the star. In Table 3, we report the uncertainties obtained for HD 4203c.

## 4. DSSI OBSERVATIONS AND DATA REDUCTION

The DSSI camera is a dual-channel speckle imaging system where each channel records speckle patterns in a different filter (Horch et al. 2009). A dichroic beamsplitter splits the white light that enters the instrument into two wavelength regimes, and then two filters further tailor the bandpasses to the desired

**Table 4**
Results of DSSI Observations

| Star | Exclusion Radius (AU) | | $5\sigma$ $\Delta m$ Limit (692 nm) | | $5\sigma$ $\Delta m$ Limit (880 nm) | |
|---|---|---|---|---|---|---|
| | Inner | Outer | 0.″1 | 0.″2 | 0.″1 | 0.″2 |
| HD 4203 | 3.86 | 108.1 | 4.87 | 5.30 | 4.53 | 5.20 |
| HD 168443 | 1.87 | 52.4 | 2.93 | 4.55 | 4.19 | 5.17 |
| HD 1690 | 15.50 | 434.0 | 4.16 | 4.64 | 3.51 | 4.59 |
| HD 137759 | 1.55 | 43.4 | 4.33 | 4.79 | 3.78 | 4.64 |

center wavelengths and widths. In the case of the observations described here, the two filters used were a red filter centered on 692 nm with a 40 nm FWHM and a near-infrared filter centered on 880 nm with a 50 nm FHWM. This setup is the same as described in Horch et al. (2012); further information regarding the magnification and the technique for measuring the pixel scale is given there.

Observations for our targets occurred on 2013 July 24–25 and 27–28. Each target was observed by taking a sequence of 1000 60 ms frames that were recorded simultaneously in each filter. The pixel format was $256 \times 256$. These data were then processed using the image reconstruction algorithms previously developed for the DSSI camera and described most recently in Howell et al. (2011). Briefly, the method is Fourier-based; we begin by computing the autocorrelation of the data frames, averaging these, and then Fourier transforming the result. The square root of this can be divided by the same result for a point source to arrive at the modulus of the object's Fourier transform. We also compute the so-called near-axis subplanes of the bispectrum (see Lohmann et al. 1983), which contain information about the derivative of the object's phase in the Fourier plane. We obtain the phase using the relaxation technique of Meng et al. (1990). The modulus and phase functions are then combined and low-pass filtered with a Gaussian filter in the Fourier plane, and the final result is inverse-transformed to give the final reconstructed image.

The goal of the DSSI observations of the objects discussed here is the detection of companion stars with sub-arcsecond separations relative to the target. The objects observed were found to be single to the limit of our detection capabilities with DSSI; to estimate the limiting magnitude as a function of separation from the target, we used the basic methodology described in Horch et al. (2011), though the image reconstruction routines have been improved somewhat since that work was completed. The result is a $5\sigma$ detection curve, showing the limiting magnitude as a function of separation, generally with increasing magnitude difference limits for larger separations.

## 5. IMAGING RESULTS

This section presents the results of the imaging observations. The reduced DSSI speckle images in the two passbands (692 nm and 880 nm) are shown in Figure 5, where the field of view is $2.8 \times 2.″8$. The limiting magnitude curves based on these images are shown in Figure 6. These show the magnitude difference between local maxima and minima in the image as a function of the separation from the central star. Also shown in these plots is a cubic spline interpolation of the $5\sigma$ detection limit from 0.″05 to 1.″2. Magnitude limits ($\Delta m$) for stellar companions compared with the magnitude of the primary are shown for separations of 0.″1 and 0.″2. These results are summarized in Table 4. We describe these separately for each of the targets and provide a more quantitative analysis of the detection limits in Section 6.

### 5.1. HD 4203

HD 4203 is a $V = 8.7$ mag dwarf star at a distance of 77.2 pc (see Table 1). The resulting $5\sigma$ detection limits shown in Table 4 and Figure 6 exclude stellar companions with $\Delta m \sim 4.5$ and $\Delta m \sim 7.5$ at separations of 0.″1 and 1.″4, respectively. These separations correspond to an exclusion range of 3.86–108.1 AU. The distance modulus for HD 4203 is −4.44. This means we can exclude the presence of M and L dwarfs at the high separation end.

### 5.2. HD 168443

HD 168443 is a $V = 6.92$ mag dwarf star and lies 37.4 pc from the Sun (see Table 1) with a distance modulus of −2.86. On the basis of the DSSI results described in this section, the presence of stellar companions with $\Delta m \sim 4.0$ and $\Delta m \sim 8.0$ are excluded at the $5\sigma$ level for separations of 0.″1 and 1.″4, respectively. These separations correspond to an exclusion range of 1.87–52.4 AU. For this target, the detection limits close to the star (0.″1) are ∼50% superior at 880 nm than at 692 nm. Additionally, detection limits at larger separations reach $\Delta m \sim 9.0$ for 880 nm. As with HD 4203, this excludes the presence of M and L dwarfs at larger separations.

Note that there is a single peak that is formally above $5\sigma$ located at 0.″7 north of the primary in the 880 nm image but not detected in the 692 nm image. A similar peak at the same location in 880 nm images was noticed for other stars during the observing run. This was caused by a light-leak problem in the 880 nm camera, which resulted in a faint reflection in the 880 nm images. A further observation of the target will confirm that this is indeed the cause of the spurious peak.

### 5.3. HD 1690

HD 1690 has the weakest exclusion limits of the four targets since is it a giant star at a larger distance. The star is a $V = 9.17$ mag K1 giant at a distance of ∼310 pc (see Table 1). The resulting distance modulus is −7.46. Our DSSI results provide $5\sigma$ stellar companion exclusion limits of $\Delta m \sim 4.0$ and $\Delta m \sim 7.5$ for separations of 0.″1 and 1.″4, respectively. These separations correspond to an exclusion range of 15.5–434 AU. This is sufficient to rule out late M dwarf stellar companions at larger separations.

### 5.4. HD 137759

HD 137759 is a bright ($V = 3.29$) K2 giant at a distance of 31 pc (see Table 1) with a distance modulus of −2.46. The $5\sigma$ detection limits resulting from our DSSI observations exclude stellar companions with $\Delta m \sim 4.0$ and $\Delta m \sim 9.0$ at separations of 0.″1 and 1.″4, respectively. These separations correspond to an

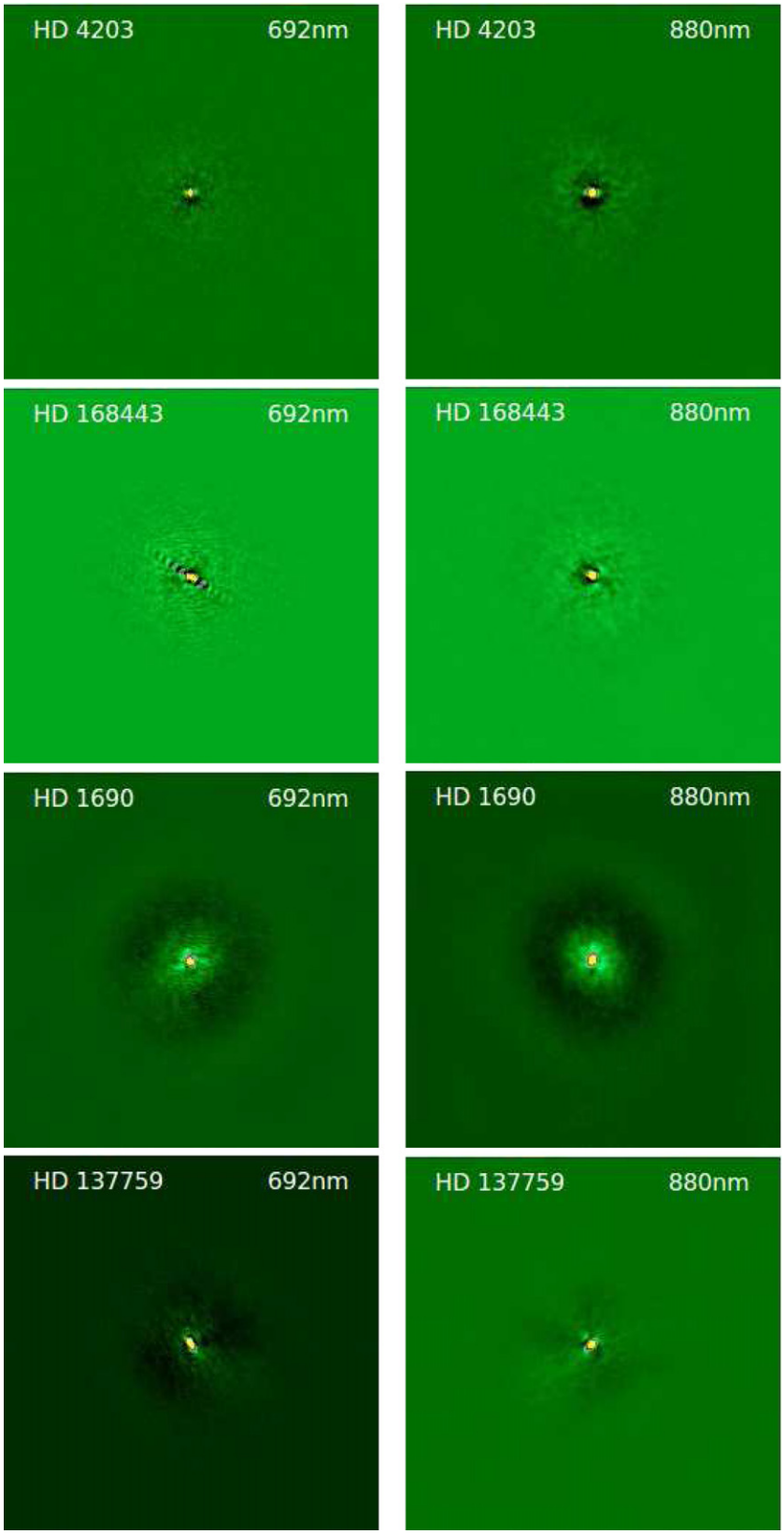


**Figure 5.** Gemini DSSI speckle images of HD 4203, HD 168443, HD 1690, and HD 137759 (iota Draconis). The left and right columns show the 692 nm and 880 nm data, respectively. The field of view is $2\farcs8 \times 2\farcs8$. For the 692 nm images, north is up and east is to the right. For the 880 nm images, north is up and east is to the left. (A color version of this figure is available in the online journal.)

exclusion range of 1.55–43.4 AU. Although this star provided the most favorable conditions for companion exclusion in terms of proximity to the star and $\Delta m$, the intrinsic brightness of the host star limits the range of stars that may realistically be excluded. On the basis of our results, we can exclude the presence of M dwarfs at large separations.

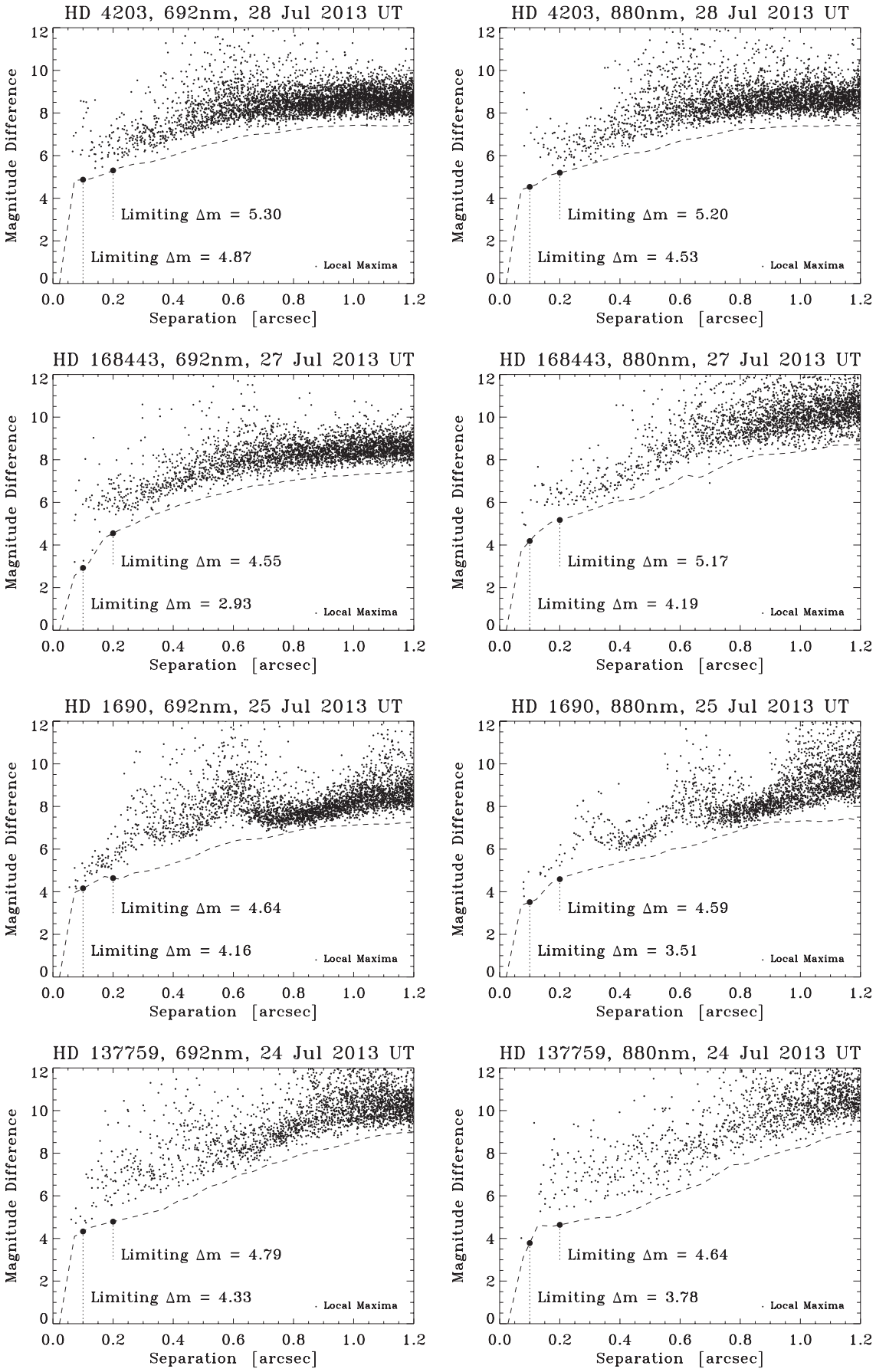


**Figure 6.** Limiting magnitude (difference between local maxima and minima) as a function of separation from the host star. Each plot was calculated from the corresponding image shown in Figure 5. The dashed line is a cubic spline interpolation of the 5$\sigma$ detection limit. Limiting magnitudes are explicitly stated for 0.″1 and 0.″2 in each case.

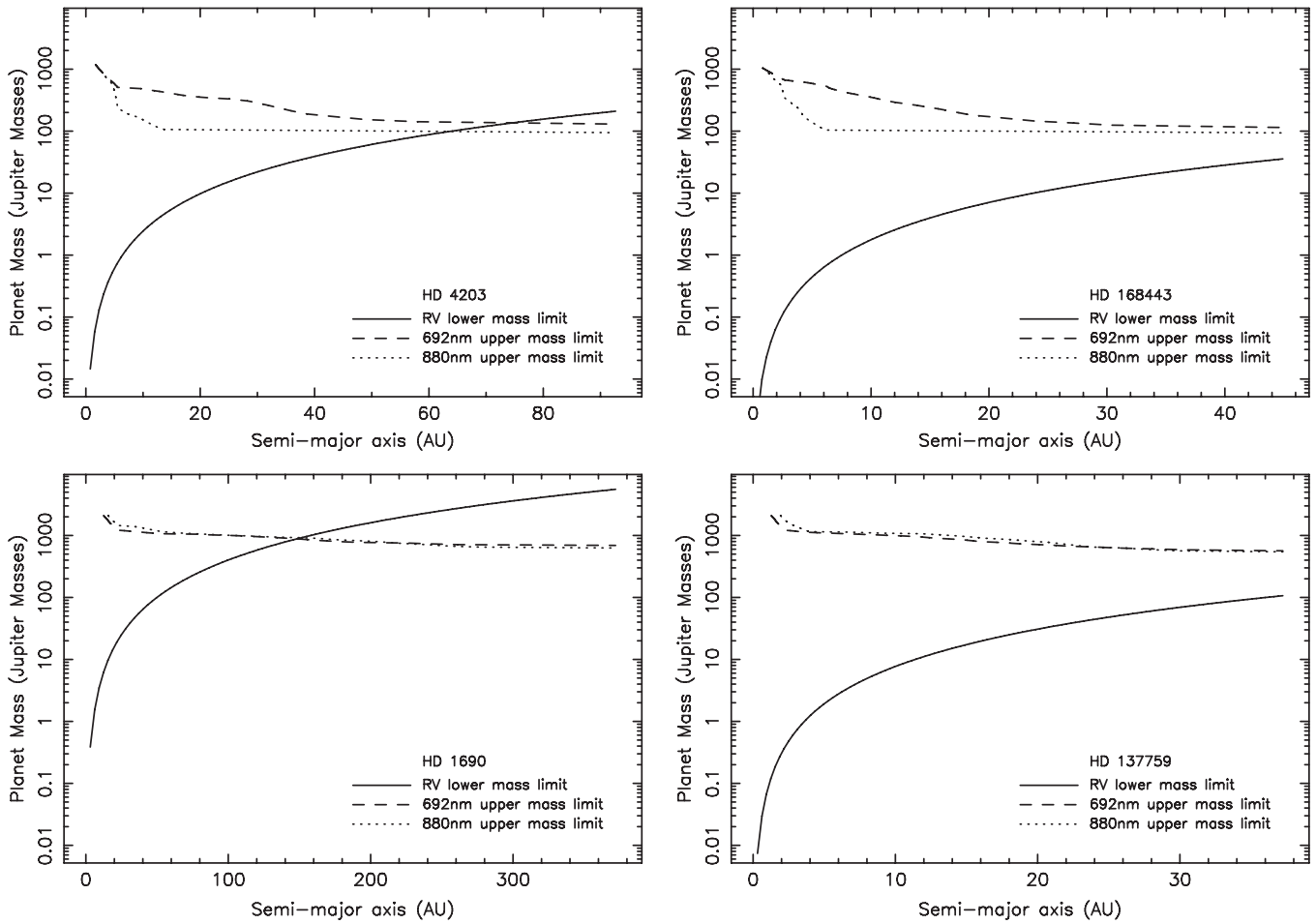


**Figure 7.** Upper and lower limits on the companion mass present in each of the four systems as a function of semi-major axis. The upper limits are calculated from the imaging results for 692 nm (dashed line) and 880 nm (dotted line). The lower limits, indicated by solid lines, are calculated based on the RV linear trends.

## 6. LIMITS TO STELLAR/PLANETARY COMPANIONS

The results presented in Section 5 provide estimates on the upper limits of stellar companions on the basis of the speckle images and distance moduli. Here we quantify both the upper and lower limits by using the speckle data results and the RV linear trends.

The conversion of the speckle $\Delta m$ values to a companion mass involved the following procedure. Since we know the mass and spectral type of the primary (see Table 1), we computed the $V$ magnitude of a possible companion as a function of spectral type and mass using the mass–radius relationship of Henry & McCarthy (1993). The resulting $\Delta V$ values were then converted to an instrumental $\Delta m$ in the two speckle filters using the Pickles spectral library and the DSSI filter transmission curves. The instrumental $\Delta m$ values for each mass were combined with the detection limit curves shown in Figure 6 to generate the limiting mass as a function of separation.

To estimate the lower limit on stellar or planetary companions to the target stars, we convert the linear trend in the RV data (shown in Table 1) to an acceleration, $\dot{v}$. The law of gravity can then be used to convert this acceleration into a mass estimate via $M_p = (\dot{v}a^2)/G$, where we have assumed a circular orbit for the companion.

The upper and lower mass limits described above are plotted for each system in Figure 7, which show companion mass as a function of separation. The upper limits derived from the 692 nm and 880 nm observations are represented by the dashed and dotted lines, respectively. The lower limits derived from the RV linear trend are shown by the solid lines. Anything below the solid curve is either not massive enough or not close enough to the host star to produce the measured RV trend. Thus, the region between the speckle curves and the RV curve are where a companion could exist at this point. Note that at larger separations, the 880 nm curve is always below the 692 nm curve, so the loss of speckle correlations in 692 nm for large separations is not relevant, as the 880 nm data tends to set the upper limit.

As described in Section 3, the linear trend is adequately explained by the presence of an additional planet. This is consistent with our null detection of a stellar companion over a broad range of separations (see Section 5). We can thus be confident that we have indeed detected a second planet in the HD 4203 system.

The two known planets of the HD 168443 system were discovered by Marcy et al. (1999, 2001). The orbital parameters were further refined by Pilyavsky et al. (2011) along with photometric observations that excluded transits for the inner planet. The revised parameters of Pilyavsky et al. (2011) also confirmed a long-term trend in the RV data that indicated the presence of a long-period companion. The DSSI results shown in Section 5 are sensitive out to a separation of 52.4 AU. The combined upper and lower mass limits shown in Figure 7 indicate that any companion within this separation range is highly likely to be planetary in nature. We thus conclude that the HD 168443 system contains a third planet for which the orbit has yet to be fully sampled with RV data.

The planet orbiting the giant star HD 1690 was discovered using HARPS data and published by Moutou et al. (2011). The DSSI observations exclude companions over a relatively broad range of separations: 15.5–434 AU. The combined mass limits shown in Figure 7 are sufficient to rule out low-mass stars only at large separations. Additionally, the companion would need to have a separation smaller than ∼20 AU in order to be of planetary mass. Thus, a stellar companion to the host star could still provide a viable explanation of the RV trend over a wide range of semi-major axis values.

The planetary companion to HD 137759 was discovered by Frink et al. (2002), and the orbit was further refined by Zechmeister et al. (2008), whose radial velocity data revealed a linear trend in the RV residuals. Further studies by Kane et al. (2010) improved the orbital parameters and confirmed the linear trend as part of the Keplerian orbital solution. Similar to HD 1690, low-mass stellar companions are ruled out at the separation limit of the DSSI observations but still possible at smaller separations.

## 7. A NOTE ON STELLAR ABUNDANCES

There have been a large number of independent studies, for example, Bond et al. (2006) and Fischer & Valenti (2005), that have consistently confirmed the enrichment of iron within giant exoplanet host stars. It is still widely debated whether the apparent increase in stellar iron content is caused by the exoplanet or whether it is a prerequisite for exoplanet formation. However, the presence of giant exoplanets leaves an undeniable tracer in the observed stellar iron abundances, where many have [Fe/H] > 0.3 dex (Santos et al. 2004).

The [Fe/H] content in HD 4203 has been measured by a number of different groups. The average [Fe/H] value is 0.41 dex, where the maximum variation between the measured abundances, or spread, is 0.06 dex (see Hinkel & Kane 2013). In other words, HD 4203 displays a classic enrichment in iron given the presence of a giant exoplanet, confirmed by multiple groups.

In comparison, HD 168443 has an average [Fe/H] abundance of 0.06 dex, with a spread in measurements of 0.18 dex between the groups. The maximum value reported was 0.12 dex by Brugamyer et al. (2011), while the lowest was −0.06 dex per Huang et al. (2005). HD 137759 had reported similar [Fe/H] measurements by four groups, where the maximum was 0.13 dex (Sadakane et al. 2005; Ecuvillon et al. 2006; Gilli et al. 2006), the minimum was −0.03 dex (Thévenin & Idiart 1999), and the average was [Fe/H] = 0.08 dex. Neither of these stars shows an obvious iron enrichment, despite the presence of giant exoplanets. Finally, given the extreme distance of HD 1690, Moutou et al. (2011) was the only source to report [Fe/H] = −0.32 dex.

Out of the four exoplanet host stars studied here, only HD 4203 exhibits iron enrichment as seen in the majority of exoplanet host stars. While HD 4203b also has the smallest eccentricity, there does not appear to be any general correlation between stellar iron content and exoplanet eccentricity (Udry & Santos 2007).

## 8. CONCLUSIONS

The stellar multiplicity of systems that harbor planets is a subject for which our knowledge base is still evolving. Its relevance plays a role in many aspects of planetary formation and evolution. Here we have presented the results of an imaging investigation of four specific systems where at least one of the planets is of high eccentricity. In all four cases we have been able to rule out the presence of all but very low-mass stars over a wide range of separations. For HD 4203, the DSSI data in combination with Keck/HIRES data confirm that there is indeed a second planet harbored in that system. We can therefore state with confidence that HD 4203 no longer has a detected RV trend without explanation. For HD 168443, the extent of the RV linear trend and the limits placed by the DSSI results strongly imply that a third planet is the best explanation for the observed trend. HD 1690 and HD 137759 are both giant stars, and so the detection limits are not quite so deep as they are for dwarfs. The DSSI results thus rule out solar-mass stars as companions to these giant hosts, but ambiguity remains as to whether a massive planet or brown dwarf at a variety of separations could explain the linear trend, although low-mass stellar companions are ruled out at large separations.

The lack of detected stellar companions in all cases returns one to the original question of determining the source of the high planetary eccentricities. The presence of a wide-binary companion has long been considered as a possible source of orbital perturbation (Zakamska & Tremaine 2004; Malmberg et al. 2007; Kaib et al. 2013). The observations presented in this work do not exclude the possibility of a stellar companion at even wider separations that may have been the catalyst for past dynamical interactions within the system. For example, the Two Micron All Sky Survey All-Sky Point Source Catalog (Skrutskie et al. 2006) does not reveal any sources within 10″ of each target. Our results also do not take into account a passing star that may have induced a similar transfer of angular momentum. A more common approach to explaining the diversity of exoplanetary eccentricities is the occurrence of past planet–planet scattering events (Adams & Laughlin 2003; Chatterjee et al. 2008; Jurić & Tremaine 2008). Given that we detect no stellar companions for our four systems, this appears to be consistent with "internal" planetary interactions.

Finally, we have shown the utility of instruments such as DSSI for conducting studies of the brightest exoplanet host stars to determine multiplicity. Continued observations will prove essential to understanding the multiplicity of exoplanet host stars that are closest to the Sun and thus place the formation our solar system and the singularity of our own star in context.

This work is based on observations obtained at the Gemini Observatory, which is operated by the Association of Universities for Research in Astronomy, Inc., under a cooperative agreement with the NSF on behalf of the Gemini partnership: the National Science Foundation (United States), the National Research Council (Canada), CONICYT (Chile), the Australian Research Council (Australia), Ministério da Ciência, Tecnologia e Inovação (Brazil), and Ministerio de Ciencia, Tecnología e Innovación Productiva (Argentina). This research has made use of the Exoplanet Orbit Database and the Exoplanet Data Explorer at exoplanets.org. This research has also made use of the NASA/IPAC Infrared Science Archive, which is operated by the Jet Propulsion Laboratory, California Institute of Technology, under contract with the National Aeronautics and Space Administration. The authors acknowledge financial support from the National Science Foundation through grant AST-1109662.

## REFERENCES

Abt, H. A., & Levy, S. G. 1976, ApJS, 30, 273
Adams, F. C., & Laughlin, G. 2003, Icar, 163, 290

Bergfors, C., Brandner, W., Daemgen, S., et al. 2013, MNRAS, 428, 182
Bond, J. C., Tinney, C. G., Butler, R. P., et al. 2006, MNRAS, 370, 163
Brugamyer, E., Dodson-Robinson, S. E., Cochran, W. D., & Sneden, C. 2011, ApJ, 738, 97
Butler, R. P., Wright, J. T., Marcy, G. W., et al. 2006, ApJ, 646, 505
Cassan, A., Kubas, D., Beaulieu, J.-P., et al. 2012, Natur, 481, 167
Chatterjee, S., Ford, E. B., Matsumura, S., & Rasio, F. A. 2008, ApJ, 686, 580
Crepp, J. R., Johnson, J. A., Howard, A. W., et al. 2012, ApJ, 761, 39
Crepp, J. R., Johnson, J. A., Howard, A. W., et al. 2013, ApJ, 774, 1
Dressing, C. D., & Charbonneau, D. 2013, ApJ, 767, 95
Duquennoy, A., & Mayor, M. 1991, A&A, 248, 485
Ecuvillon, A., Israelian, G., Santos, N. C., Mayor, M., & Gilli, G. 2006, A&A, 449, 809
Eggenberger, A., Udry, S., Chauvin, G., et al. 2007, A&A, 474, 273
Eggenberger, A., Udry, S., & Mayor, M. 2004, A&A, 417, 353
Fischer, D. A., & Valenti, J. 2005, ApJ, 622, 1102
Frink, S., Mitchell, D. S., Quirrenbach, A., et al. 2002, ApJ, 576, 478
Gilli, G., Israelian, G., Ecuvillon, A., Santos, N. C., & Mayor, M. 2006, A&A, 449, 723
Henry, T. J., & McCarthy, D. W., Jr. 1993, AJ, 106, 773
Hinkel, N. R., & Kane, S. R. 2013, MNRAS, 432, L36
Horch, E. P., Gomez, S. C., Sherry, W. H., et al. 2011, AJ, 141, 45
Horch, E. P., Howell, S. B., Everett, M. E., & Ciardi, D. R. 2012, AJ, 144, 165
Horch, E. P., Veillette, D. R., Baena Galle, R., et al. 2009, AJ, 137, 5057
Howell, S. B., Everett, M. E., Sherry, W., Horch, E., & Ciardi, D. R. 2011, AJ, 142, 19
Huang, C., Zhao, G., Zhang, H. W., & Chen, Y. Q. 2005, MNRAS, 363, 71
Jurić, M., & Tremaine, S. 2008, ApJ, 686, 603
Kaib, N. A., Raymond, S. N., & Duncan, M. 2013, Natur, 493, 381
Kane, S. R., Reffert, S., Henry, G. W., et al. 2010, ApJ, 720, 1644
Lohmann, A. W., Weigelt, G., & Wirnitzer, B. 1983, ApOpt, 22, 4028
Malmberg, D., de Angeli, F., Davies, M. B., et al. 2007, MNRAS, 378, 1207
Marcy, G. W., Butler, R. P., Vogt, S. S., et al. 2001, ApJ, 555, 418
Marcy, G. W., Butler, R. P., Vogt, S. S., Fischer, D., & Liu, M. C. 1999, ApJ, 520, 239
Meng, J., Aitken, G. J. M., Hege, E. K., & Morgan, J. S. 1990, JOSAA, 7, 1243
Moutou, C., Mayor, M., Lo Curto, G., et al. 2011, A&A, 527, 63
Pilyavsky, G., Mahadevan, S., Kane, S. R., et al. 2011, ApJ, 743, 162
Press, W. H., Teukolsky, S. A., Vetterling, W. T., & Flannery, B. P. 2002, in Numerical Recipes in C++: The Art of Scientific Computing, ed. W. H. Press (Cambridge: Univ. of Cambridge), 002
Raghavan, D., McAlister, H. A., Henry, T. J., et al. 2010, ApJS, 190, 1
Roell, T., Neuhäuser, R., Seifahrt, A., & Mugrauer, M. 2012, A&A, 542, 92
Sadakane, K., Ohnishi, T., Ohkubo, M., & Takeda, Y. 2005, PASJ, 57, 127
Santos, N. C., Israelian, G., & Mayor, M. 2004, A&A, 415, 1153
Skrutskie, M. F., Cutri, R. M., Stiening, R., et al. 2006, AJ, 131, 1163
Thévenin, F., & Idiart, T. P. 1999, ApJ, 521, 753
Udry, S., & Santos, N. C. 2007, ARA&A, 45, 397
van Leeuwen, F. (ed.) 2007, Hipparcos, the New Reduction of the Raw Data, Astrophysics and Space Science Library, Vol. 350 (Dordrecht: Springer)
Vogt, S. S., Allen, S. L., Bigelow, B. C., et al. 1994, Proc. SPIE, 2198, 362
Vogt, S. S., Butler, R. P., Marcy, G. W., et al. 2002, ApJ, 568, 352
Wang, S. X., Wright, J. T., Cochran, W., et al. 2012, ApJ, 761, 46
Wright, J. T., Fakhouri, O., Marcy, G. W., et al. 2011, PASP, 123, 412
Wright, J. T., & Howard, A. W. 2009, ApJS, 182, 205
Zakamska, N. L., & Tremaine, S. 2004, AJ, 128, 869
Zechmeister, M., Reffert, S., Hatzes, A. P., Endl, M., & Quirrenbach, A. 2008, A&A, 491, 531
Zucker, S., & Mazeh, T. 2002, ApJL, 568, L113